González Suárez, A.; Trujillo Guillen, M.; Koruth, J.; D'avila, A.; Berjano, E. (2014). Radiofrequency cardiac ablation with catheters placed on opposing sides of the ventricular wall: Computer modelling comparing bipolar and unipolar modes. International Journal of Hyperthermia. 30(6):372-384. doi:10.3109/02656736.2014.949878.

FINAL VERSION

Radiofrequency cardiac ablation with catheters placed on opposing sides of the ventricular wall: computer modeling comparing bipolar and unipolar modes

Ana González-Suárez[1], Macarena Trujillo[2], Jacob Koruth[3], Andre d'Avila[3*], and Enrique Berjano[1]

[1]*Biomedical Synergy, Electronic Engineering Department, Universitat Politècnica de València, Spain*

[2]*Instituto Universitario de Matemática Pura y Aplicada, Universitat Politècnica de València, Spain*

[3] *Helmsley Cardiac Electrophysiology Center, Mt Sinai Medical New York, NY, USA*

[*]*Current affiliation: Hospital Cardiologico, Florianopolis, Santa Catarina, Brazil*

Address for correspondence:

Ana González-Suárez

Biomedical Synergy, Electronic Engineering Department (Building 7F)

Universitat Politècnica de València, Spain

Camino de Vera, 46022 Valencia, Spain

Phone: 34–963877607, Fax: 34–963877609

Email: angonsua@eln.upv.es

Short title: Bipolar and unipolar ventricular RF ablation

Abstract

Purpose: To compare the efficacy of bipolar (BM) versus unipolar (UM) mode of radiofrequency ablation (RFA) in terms of creating transmural lesions across the interventricular septum (IVS) and ventricular free wall (VFW).

Materials and methods: We built computational models to study the temperature distributions and lesion dimensions created by BM and UM on IVS and VFW during RFA. Two different UM types were considered: sequential (SEUM) and simultaneous (SIUM). The effect of ventricular wall thickness, catheter misalignment, epicardial fat, and presence of air in the epicardial space were also studied.

Results: As regards IVS ablation, BM created transmural and symmetrical lesions for wall thicknesses up to 15 mm. SEUM and SIUM were not able to create transmural lesions with IVS thicknesses ≥ 12.5 and 15 mm, respectively. Lesions were asymmetrical only with SEUM. For VFW ablation, BM also created transmural lesions for wall thicknesses up to 15 mm. However, with SEUM and SIUM transmurality was obtained for VFW thicknesses ≤ 7.5 and 12.5 mm, respectively. With the three modes VFW lesions were always asymmetrical. In the scenario with air or a fat tissue layer on the epicardial side, only SIUM was capable of creating transmural lesions. Overall, BM was superior to UM in IVS and VFW ablation when the catheters were not aligned.

Conclusions: Our findings suggest that BM is more effective than UM in achieving transmurality across both ventricular sites, except in the situation of the epicardial catheter tip surrounded by air or placed over a fat tissue layer.

Keywords*: bipolar ablation, interventricular septum, radiofrequency ablation, unipolar ablation, ventricular ablation, ventricular free wall.*

Introduction

Successful radiofrequency ablation (RFA) of ventricular tachycardia (VT) originating from sites within the left ventricle such as the interventricular septum (IVS) is often limited by the presence of deep intramural circuits. The creation of such deep lesions while needed, cannot be always achieved with unipolar mode (UM) of RF ablation. Recent experimental studies have shown that using two catheters placed on opposing IVS surfaces to deliver RF in the bipolar mode (BM) allows deeper lesions to be created [1,2]. These results suggest that BM could be more effective than UM at eliminating VTs from deep intramural sites. However, the effects of different ventricular wall thicknesses and catheter alignment on the degree of transmurality and lesion geometry created have never been studied in detail. Although, BM and UM have previously been compared in the ventricular free wall (VFW) ablations [3-5], no information is available on their performance in an endocardium–epicardium approach. A recent study by Nagashima *et al.* [6] did consider this approach, but the effects of the above-mentioned factors were not included.

Our aim was to assess by means of computer modeling the thermal lesions created in the ventricular wall, in particular the degree of transmurality achieved, in a comparison of BM and two different UM (sequential unipolar mode, SEUM and simultaneous unipolar mode, SIUM). As far as we know, there has not yet been a published study using a computational model to compare these ablation strategies. Two and three-dimensional computational models were therefore developed and simulations were conducted to investigate temperature distribution and lesion geometry during RFA of the IVS (i.e. endocardium–endocardium approach) and VFW (i.e. endocardium–epicardium approach). The effect of wall thickness, catheter misalignment, the presence of air in the epicardial space and fat on the epicardial side were also studied. Although

as a rule the epicardial space does not contain any air, during epicardial puncture and instrumentation, small amounts of air may accumulate around the ablation catheter.

Materials and methods

Computer modeling

Numerical models were based on a coupled electric-thermal problem which was solved numerically using the Finite Element Method (FEM) with COMSOL Multiphysics software (COMSOL, Burlington MA, USA). The governing equation for the thermal problem was the Bioheat Equation [7] which was modified by the enthalpy method [8, 9] incorporating the phase change to model tissue vaporization:

$$\frac{\partial(\rho h)}{\partial t} = \nabla \cdot (k \nabla T) + q - Q_p + Q_m \tag{1}$$

where ρ is density (kg/m^3), h enthalpy, t time (s), k thermal conductivity (W/m·K), T temperature (ºC), q the heat source caused by RF power (W/m^3), Q_p the heat loss caused by blood perfusion (W/m^3) and Q_m the metabolic heat generation (W/m^3). Q_p and Q_m were not considered since the former can be ignored in the case of cardiac ablation (far from large vessels) [10] and the latter is negligible in comparison to the other terms [7]. In biological tissues enthalpy is related to tissue temperature by the following expression [8, 11]:

$$\frac{\partial(\rho h)}{\partial t} = \frac{\partial T}{\partial t} * \begin{cases} \rho_l c_l & 0 < T \le 99^o C \\ h_{fg} C & 99 < T \le 100^o C \\ \rho_g c_g & T > 100^o C \end{cases} \tag{2}$$

where ρ_i and c_i are the density and specific heat of cardiac tissue before phase-change ($i=l$) and post-phase-change ($i=g$), respectively; h_{fg} is the latent heat and C the tissue water content. We considered a latent heat value of $2.162 \cdot 10^9$ J/m^3, which corresponds

to the product of the water vaporization latent heat and the water density at 100ºC, and a tissue water content of 75% inside the cardiac tissue.

The thermal lesions created in the ventricular wall were assessed using the Arrhenius damage model [12-15], which associates temperature with exposure time using a first order kinetics relationship:

$$\Omega(\tau) = \ln\left\{\frac{C(0)}{C(\tau)}\right\} = \int_0^{\tau} A e^{\frac{-E_a}{RT(t)}} dt \tag{3}$$

where $\Omega(\tau)$ is the degree of tissue injury, τ the total heating time (s), $C(\tau)$ the present concentration of living cells, $C(0)$ the initial concentration of living cells, R the universal gas constant, A the frequency factor (s^{-1}), and E_a the activation energy for the irreversible damage reaction (J/mol). The tissue damage integral is associated with the percentage volume of cells surviving uniform exposure to a given temperature for a certain length of time. For instance, damage integral $\Omega = 1$, which corresponds to a viable cell concentration of 37%, means there is a 63% probability of cell death. The parameters A and E_a are dependent on tissue type; for the cardiac tissue we considered those proposed by Jacques and Gaenni [16]: $A = 2.94 \cdot 10^{38}\ s^{-1}$ and $E_a = 2.596 \cdot 10^5$ J/mol. These values are derived from experiments in which an assessment was made of the changes in tissue optical properties caused by heating, and hence are not directly related to damage at the cellular level, i.e. $\Omega = 1$ does not necessarily mean there is exactly a 63% probability of cell death. However, $\Omega = 1$ can be used to compare the thermal lesions created by the three ablation modes.

At the RF frequencies (≈500 kHz) used in RF heating and over the distance of interest, the biological medium can be considered almost totally resistive, since the displacement currents are much less important than conduction currents. This means a quasi-static approach can be used to solve the electrical problem [17]. The distributed heat source q is then given by $q = \sigma|\boldsymbol{E}|^2$, where $|\boldsymbol{E}|$ is the magnitude of the vector

electric field (V/m) and σ is electrical conductivity (S/m). $\boldsymbol{E}$ is calculated from $\boldsymbol{E} = -\nabla\Phi$, where Φ is the voltage (V), which is obtained by solving Laplace's equation, which is the governing equation of the electrical problem:

$$\nabla \cdot (\sigma \nabla \Phi) = 0 \tag{4}$$

The models considered two internally cooled catheter tip electrodes (7Fr diameter, 4 mm catheter tip), similar to those used in RF cardiac ablation [3, 4, 18, 19]. Although open-irrigated catheters are commonly used for VFW ablation [6], they have been associated with problems of fluid accumulation in the epicardial space (due to saline irrigation) necessitating frequent aspirations before each lesion [20]. The volume of fluid infused into the epicardial space may also alter the biophysical properties of the pericardial fluid [3] and interfere with catheter–tissue contact, leading to inadequate lesion formation [20].

Figure 1 shows the model geometry for the IVS ablation case, i.e. both electrodes placed perpendicularly to the septum surfaces (endocardium–endocardium approach) and surrounded by circulating blood. Since the region under study has axial symmetry, a two-dimensional model was used. In the case of VFW ablation (endocardium–epicardium approach), the epicardial catheter is surrounded by pericardial fluid, and hence this approach was modeled by replacing the circulating blood with pericardial fluid on the epicardial side (not shown in Figure 1). We have also conducted additional computer simulations in which the pericardial fluid was replaced by air. The simulation of air around the epicardial catheter is important, since small amounts of air could be inadvertently introduced during epicardial puncture or during catheter manipulation during the procedure. Our simulations represented a worst-case scenario in which the electrode is completely surrounded by air. We also studied the influence of overlying epicardial fat tissue on lesion formation, considering an epicardial fat layer with a

typical thickness of 2.6 mm [3] between the epicardial catheter tip and the target site (i.e. the VFW). In these simulations the epicardial space was filled with pericardial fluid, since this is the normal scenario.

Ventricular wall thickness (IVS or VFW) was varied between 5 and 15 mm. Ventricle dimensions X= Z = 40 mm were estimated by means of a convergence test in order to avoid boundary effects, using as control parameter the value of the maximal temperature achieved in the tissue (T_{max}) after 120 s of heating. We first considered a tentative spatial (i.e. minimum meshing size) and temporal resolution. To determine the appropriate parameters of X and Z, we increased their values by equal amounts. When the difference in the T_{max} between consecutive simulations was less than 0.5%, we considered the former values to be adequate. We then determined adequate spatial and temporal resolution by means of similar convergence tests using the same control parameter as in the previous test. Discretization was spatially heterogeneous: the finest zone was always the electrode-tissue interface, where the largest voltage gradient was produced and hence the maximum value of current density. In the tissue, grid size was increased gradually with distance from the electrode-tissue interface. The convergence tests provided a grid size of 0.2 mm in the finest zone (electrode-tissue interface) and a step time of 0.05 s.

We also built three-dimensional (3D) models, which were used to represent a scenario in which the two electrodes were not aligned exactly opposite to each other. These 3D models also allowed for simulation of parallel placement of the epicardial catheter tip (as opposed to perpendicular) to the epicardium during VFW ablation, as is usual in clinical practice.

The thermal and electrical properties of the model elements are shown in Table I [21-24]. Due to the lack of information on the electrical and thermal characteristics of

the pericardial fluid we assumed it to have the same characteristics as saline [22] as a first approximation. The electrical (σ) and thermal conductivity (k) of the cardiac tissue were temperature-dependent functions and were defined by piecewise functions. For σ we considered an exponential growth of 1.5%/ºC up to 100ºC [21] and then a drop of 4 orders for five degrees to model the desiccation process [25], while k grew linearly 0.12%/ºC up to 100ºC, after which temperature k was kept constant [7].

Figure 2 shows the electrical and thermal boundary conditions applied to the model. The BM (Figure 2(a)) was electrically modeled with an electrical isolation boundary condition set at the model limits and a voltage drop of 40 V (which corresponds to 16 W, considering impedance of 100 Ω) applied between the two electrodes throughout the total ablation time of 120 s, so that the electrical currents were always forced to flow between both electrodes. In the SEUM (Figure 2(b)), a constant zero voltage was always set at the model limits (mimicking the electrical performance of the dispersive electrode) and one of the active electrodes was set at 40 V while another was electrically isolated for the first 60 s. These conditions were reversed for the subsequent 60 s, which gave a total ablation time of 120 s. In the SIUM (Figure 2(c)), as in the previous mode, the limits of the model were fixed at 0 V (dispersive electrode), while both electrodes were set at 40 V during the total ablation process of 120 s, so that the electrical currents were forced to flow simultaneously between each catheter and the dispersive electrode. The voltage applied in all the ablation modes was chosen to keep the catheter tip temperature below 42ºC [3, 20], as is the usual clinical practice with this type of electrode. All unipolar and bipolar ablations were performed for a total duration of 120 s, as in previous studies [1, 2, 6, 26].

Thermal boundary conditions (Figure 2(d)) were a null thermal flux on the symmetry axis and a constant temperature of 37ºC (T_{body}) on the surfaces at a distance

from the active electrode. The cooling effect produced by the blood circulating inside the ventricles (T_{blood} = 37ºC) was modeled by means of two forced thermal convection coefficients in the endocardium–blood ($h_{CL} = h_{CR}$) and electrode–blood ($h_{EL} = h_{ER}$) with a value of 708 W/m^{2}K and 3636 W/m^{2}K, respectively [21]. In the VFW model, we considered a free thermal convection coefficient in the epicardium–air/pericardial fluid interface of 20 W/m^{2}K. The cooling effect produced by the fluid circulating inside the electrode was not modeled realistically by means of internal tubes (the electrodes were empty, as shown Figure 1), but with a forced thermal convection coefficient (h_i) of 10629 W/m^{2}K and a coolant temperature of 21ºC (room temperature). The value of this coefficient was estimated by using the theoretical calculation of forced convection inside a tube [27]. We considered an internal flow rate of 36 mL/min [3] and half of the tube cross section (1.3 mm^2).

Results

Interventricular septum ablation

Figure 3 shows the temperature distributions and lesion shapes in the IVS after RFA, considering different septum thickness and the three ablation modes. The solid black line indicates the thermal damage borderline (Ω = 1) and therefore outlines the lesion. Table II shows the lesion dimensions shown in Figure 3.

The lesions created in the IVS using BM (Figure 3(a)) were always transmural and symmetrical when the septum wall was between 5 and 15 mm thick, although their geometry differed slightly with thickness. When IVS was ≤ 10 mm, the maximum lesion width occurred in the middle of the septum, while for IVS ≥ 12.5 mm the lesion had an hourglass shape, with the minimum width at the middle of the septum.

The lesion shapes in the case of SEUM (Figure 3(b)) differed significantly from those obtained with BM. The most significant finding was that it was not possible to create transmural lesions for septum thicknesses ≥ 12.5 mm and lesions were asymmetrical. When the septum thickness was 15 mm, one would expect two identical lesions to be created independently due to the large distance between electrodes. However, the lesions remained asymmetrical. In fact, the lesion depth around the first activated electrode (left ventricular side) was 3.70 mm, as compared to 5.01 mm on the right ventricular side, where the electrode was the second to be activated. The lesions were also found to be in general wider around the secondly activated electrode (right ventricular side) (see surface and maximum widths in Table II).

The lesion shapes in the case of SIUM are shown in Figure 3(c). As in BM, the lesions were symmetrical for all thicknesses considered. However, in this case, it was not possible to create transmural lesions for thicknesses ≥ 15 mm.

Ventricular free wall ablation

Figure 4 shows the temperature distributions and lesion shapes in the VFW after RFA, considering different ventricular thicknesses and the three ablation modes. Table III gives the dimensions of these lesions.

The lesions created with BM were transmural for thicknesses up to 15 mm, as shown in Figure 4(a) and lesion shape varied according to the thickness. For VFW ≤ 10 mm, the maximum lesion width occurred in the middle of the ventricular wall (which has the same width as the epicardial surface), while for VFW ≥ 12.5 mm the lesion had an hourglass shape, with the minimum width at the middle of the ventricular wall. However, unlike IVS ablation, the lesions were never symmetrical and were slightly wider around the electrode placed on the epicardium (right side).

The SEUM was only able to create transmural lesions when the VFW was ≤ 7.5 mm (Figure 4(b)). The lesions were always asymmetrical and considerably larger on the epicardial side, regardless of ventricular wall thickness. The most important difference with the IVS case was that the lesion width on the epicardial side was much larger.

With SIUM it was possible to create transmural lesions for VFW ≤ 12.5 mm (Figure 4(c)). The lesion shapes were always asymmetrical and wider around the electrode placed on the epicardium, unlike the IVS ablation.

Effect of air on the epicardial side

We assessed the effect of the accidental presence of air around the epicardial catheter tip. Figure 5 shows the temperature distributions and lesion geometries in the VFW (10 mm thickness) using the three modes of ablation. The most important finding was the absence of a thermal lesion on the endocardial side with BM (Figure 5(a)). SEUM also failed to create transmural lesions, although a lesion did form on the endocardial side (see Figure 5(b)). The lesions created on each side of the wall had similar shapes, with a depth and width of approximately 4 mm and 7 mm, respectively. SIUM was the only technique capable of creating a transmural lesion, which was symmetrical in the shape of an hourglass (see Figure 5(c)).

Effect of overlying fat tissue on the epicardial side

We also studied the effect of the presence of overlying fat tissue on the epicardial side. Figure 6 shows the temperature distributions and lesion geometries in the VFW (10 mm thickness) for the three modes of ablation. It is important to note that the lesions in the epicardial fat layer were created by thermal conduction from the heated pericardial fluid in all three ablation modes, and not by direct RF heating. Due to the

overheating of the pericardial fluid, water vaporization had to be calculated by the enthalpy method (Eq. 2). We assumed that the pericardial fluid was composed of water only (with characteristics as in the case of aqueous humor [9]). The temperature in the pericardial fluid was thus below 111ºC, as can be seen in Figure 6.

We observed that it was not possible to create transmural lesions in BM, not even the lesion on the epicardial side reached the cardiac wall tissue (see Figure 6(a)). The lesion on the endocardial side had a depth and width of approximately 4 mm and 6 mm, respectively. Nor was SEUM able to create transmural lesions, although a lesion with a depth of ≈ 3 mm was created in the cardiac wall on the epicardial side (see Figure 6(b)). The lesion on the endocardial side was larger than with BM, with a depth and a width of ≈ 5 mm and 10 mm, respectively. In contrast, SIUM was the only mode capable of creating a transmural lesion, which had an hourglass shape and was wider around the epicardial side (see Figure 6(c)).

Effect of changing the orientation of epicardial catheter

We also assessed the effect of changing the orientation of the epicardial catheter tip from perpendicular to parallel, as is usual in clinical practice. We used a 3D model due to the lack of axial symmetry in this situation. The BM ablation and pericardial fluid in the epicardial space were considered since it was the best scenario in which transmural lesions were achieved. Figure 7 shows the temperature distributions and lesion shapes in the VFW (10 mm thickness) with BM. The lesion shapes in both situations were almost identical, which suggests that the orientation of the epicardial catheter tip does not have a significant effect on lesion geometry.

Effect of the misalignment of catheters

We assessed the effect of the progressive misalignment of the catheters on lesion dimension and transmurality in both IVS and VFW. Only BM and SIUM were considered since we had seen that they were superior to SEUM in creating transmural lesions in both scenarios. Catheter misalignment was varied in steps of 2.5 mm from 0 mm (no misalignment) until the lesion was no longer transmural. The temperature distributions and lesion geometries in the IVS and VFW (both 10 mm thickness) with BM and SIUM are shown in Figures 8 and 9, respectively.

In general, the lesions were seen to become longer as misalignment increased and the lesion shape became more hourglass-like. BM was superior to SIUM in IVS ablation, since it was capable of creating transmural lesions up to a catheter misalignment of 10 mm. The lesions were always symmetrical in IVS ablation, regardless of ablation mode and catheter misalignment (see Figure 8). In the case of VFW ablation, BM was also more effective than SIUM in creating transmural lesions, which happened until catheter misalignment reached 12.5 mm, as shown in Figure 9. Unlike IVS ablation, the lesions were asymmetrical and wider on the epicardial surface and were even wider with SIUM.

Discussion

Our objective was to compare the efficacy of BM and two different UM (SEUM and SIUM) in RF cardiac ablation. Specifically we attempted to look at their ability to create transmural lesions across ventricular tissue in two locations: 1) across the IVS with the electrodes located on either side of the septum, and 2) across the VFW with one electrode located on the endocardial side of the ventricle and the other on its epicardial surface.

The computer modeling results demonstrated that BM created larger lesions than SEUM and SIUM across the IVS (see Figure 3). These findings are in agreement with those obtained in previous experimental studies on bipolar ablation of the IVS. Nagashima *et al.* [2] compared BM and SEUM using saline-irrigated electrodes on excised swine hearts and found that BM produced a higher number of transmural lesions. Sivagangabalan *et al*. [1] also found that BM required fewer ablations to achieve block across ablation lines and created larger lesions in a post infarct ovine model. It is worthy of note that in this study we found the upper transmurality limit when using BM (40 V/120 s) across IVS thicknesses up to 15 mm. Although this was assessed using the above parameters in computer modeling, this conclusion is relevant when one is targeting hypertrophied left ventricular myocardium. Interestingly, we also observed that lesions were not symmetrical during SEUM; the lesions were in general larger (in depth and width) on the side of the second activated catheter. This was due to the result of higher electrical conductivity on the site of the lesion created around the second activated catheter, due to residual heating from the preceding lesion (electrical conductivity at a given point is inversely proportional to the absorbed RF power and hence to heating) and likely facilitates the deposition of more RF power. This was confirmed by conducting additional simulations with constant electrical conductivity in the tissue. We found that under these circumstances the lesions obtained were practically symmetrical. Overall, the difference in thermal dosage may seem negligible, but our results suggest that this could be significant and may explain the differences in the SEUM lesions in previous experimental results [1].

Our results also suggest that BM creates larger lesions than both UM across the VFW (see Figure 4), with the lesions being always asymmetrical. This is true as long as the epicardial catheter tip is not surrounded by air or placed over an epicardial fat layer,

as shown in Figure 5 and 6. The results show that in the first situation (with air in the epicardial space), BM produces a thermal lesion only on the epicardial side, making transmurality unlikely (Figure 5). This is due to the large difference in electrical current density between the catheter tips, i.e. on the epicardial side the electrode would have limited contact with the tissue, resulting in a lower effective contact area and hence a higher current density; while on the other hand the endocardial catheter which would be completely surrounded by cardiac tissue and blood (the electrical conductivity of blood is even higher than cardiac tissue) resulting in a lower current density. As the RF power absorbed by the tissue (directly converted into heat) is directly proportional to the square of current density, lesions will be preferentially (or even exclusively) created around the epicardial catheter tip due to its high current density, as opposed to on the endocardial surface. In other words, when air is present around the epicardial catheter tip BM should not be considered as a pure bipolar mode across the VFW. In fact, the temperature distribution shown in Figure 5(a) suggests that the electrode on the epicardium actually behaves as a single active electrode, whereas the electrode on the endocardium plays the role of a dispersive electrode, thus giving negligible heating in its vicinity (definition of unipolar mode). SIUM is therefore likely to be more effective than BM in achieving transmural lesions under this condition (see Figure 5(c)), at least for wall thicknesses up to 10 mm. From a practical point of view, the presence of air around the epicardial catheter tip could be checked pre-ablation by measuring the unipolar impedances, i.e. between the epicardial electrode and the patch. A much higher value than that found between the endocardial electrode and the patch would suggest the presence of air or suboptimal conditions, favoring non transmural lesions.

Regarding the situation with a fat layer on the epicardial side, the results show that in all three ablation modes the lesions in the epicardial fat layer were created by thermal

conduction of the heated pericardial fluid from the epicardial surface (Figure 6). This was due to the electrical conductivity of fat tissue being lower than that of the pericardial fluid (see Table I), which meant that the RF currents preferably flowed through the pericardial fluid instead of the fat tissue. Under these circumstances, we observed that SIUM was more effective than BM in achieving transmural lesions (see Figure 6(c)), since both catheters were applying energy at the same time during ablation. In fact, BM was not able to create a lesion in the cardiac wall tissue on the epicardial side (Figure 6(a)).

We also observed some cases of tissue temperature reaching around 110ºC. This value can lead to the formation and expansion of steam and even to disruption of the tissue surface. This undesirable effect is known as “steam popping” [19]. Our results suggest that this effect would be more pronounced with unipolar modes, especially SEUM, in which overall temperatures reached higher values. As can be seen in Figure 3, SEUM was the only mode in which the IVS temperature on the right ventricular side reached ≈110ºC. For VFW ablation (see Figure 4), the temperature in the tissue around the epicardial catheter tip was higher with both unipolar modes (SEUM and SIUM). Our results therefore suggest that BM would be safer than unipolar modes on both ventricular sites in terms of avoiding tissue popping.

The effect of changing the orientation of the catheter tip to the epicardial surface (from perpendicular to parallel) on lesion development during VFW bipolar ablation seems to be insignificant as suggested by the results shown in Figure 7.

We also observed that BM was superior to UM in IVS and VFW ablation when both catheters were misaligned, as shown in Figures 8 and 9. In the case of VFW ablation, transmurality was maintained up to a misalignment of 12.5 mm between electrodes, while in IVS ablation transmurality was maintained only up to 10 mm

misalignment. This is due to more power being lost in bipolar IVS ablation from heat removal by circulating blood.

Overall, we observed that SEUM was the least effective method in terms of creating transmural lesions. In Figures 3 and 4 it can be seen that SEUM was the only mode not able to create transmural lesions in 12.5 mm thick IVS and VFW after 120 s of RFA. In order to assess whether the effectiveness of SEUM could be improved by increasing RFA duration on each site on the ventricular wall, we conducted additional simulations considering the cases of IVS and VFW with a thickness of 12.5 mm and increasing the duration to 120 s on each side of the ventricular wall, i.e. a total duration of 240 s. As can be seen in Figure 10, doubling the ablation time made it possible to create transmural lesions with SEUM, which suggests that this method could be just as effective as the other methods when the duration is increased on each side of the ventricular walls.

Study Limitations

Our study used has certain limitations. We modeled an internally-cooled catheter, and although these catheters are used for clinical RF ablation of cardiac tissue [3, 4, 18, 19], other types of catheters, such as non-irrigated and open-irrigated catheters, are also employed for this type of intervention. The conclusions reached in this study could therefore be different when using other catheter designs. For example in the case of VFW ablation with the epicardial catheter tip surrounded by air, Nagashima *et al.* [6] used an open-irrigated catheter only on the epicardial side. Our results suggest that this approach would improve the efficacy of BM, since saline irrigation is a conductive solution and would increase the effective contact area in the epicardial space. Similarly,

in the case of overlying epicardial fat, the saline would change the biophysical properties of the epicardial fat tissue to give higher electrical conductivity.

In addition, although different lesions could be created when considering: a) different insertion depths of the catheter tip into tissue and b) different voltage/time settings, it is likely that the above conclusions regarding the impact on the lesion geometry of BM vs. UM, ventricular wall thickness, and misalignment between electrodes will remain essentially unchanged. The results could be also different using other values of applied voltage. For instance, in the case of SEUM, a higher voltage in the first activated (upper) catheter and lower in the second could enhance the lesions made by the first catheter. Moreover, it is important to point out that our study modeled a SIUM based on a voltage applied simultaneously through both electrodes, which is equivalent to using a single RF generator. Otherwise, a SIUM in which two independent RF generators are delivering two voltage signals "isolated from one another" could also provide different results.

It is also important to point out that the thermal lesion boundaries were computed from parameters A and E_a (see Eq. 3), which are derived from optical changes in the tissue caused by heating and not from changes in cellular response. As far as we know, there are no experimental data in existence of A and E_a for cardiac tissue that quantifies the changes in cellular response caused by heating. The only available data are derived exclusively from optical changes [16, 28]. The consequences of this can be observed when the location of the isoline $\Omega = 1$ in our results is compared to the location of the isotherms. For instance, in Figure 7 the $\Omega = 1$ contour approximately matches the 60ºC isotherm instead of the values between 50ºC and 56ºC, which are usually considered to represent the isotherms of irreversible myocardial injury in hyperthermic ablation [29]. This is in agreement with the findings by Wood e*t al.* [30], in which the discoloration

zone in the cardiac tissue matched the ~60ºC isotherm. Although Wood e*t al.* [30] concluded that the lethal isotherm for cardiac myocardium is near 61ºC, the staining procedure they used to measure the area of acute necrosis has been criticized for underestimating the extent of irreversible tissue injury [29]. Although we are aware that our results could be different whether we had considered other Arrhenius parameters or a 50ºC isotherm to assess the thermal lesions, the aim of our study was not to exactly predict lesion size, but to compare the effectiveness of bipolar versus unipolar modes in terms of their capacities to create transmural lesions across both ventricular walls. For this reason, using the $\Omega = 1$ contour, even when computed from parameters derived from optical changes, allowed a comparison of the three ablation modes.

Finally, our computational models could be refined to include blood velocity in the ventricles, rather than using forced convection coefficients. In any case, it is generally accepted that this aspect would not affect either the temperature distribution in the tissue or the lesions created in the ventricular wall, but would provide a more realistic temperature distribution in the blood [31].

Conclusions

Our findings, under the simulated conditions, suggest that bipolar RF cardiac ablation on the interventricular septum and ventricular free wall is superior to both unipolar modes in terms of achieving lesion transmurality across ventricular walls. This holds true even when the catheters are misaligned, as can occur in clinical practice. The two situations in which bipolar is inferior to unipolar mode are in the case of ventricular free wall ablation, when the epicardial catheter tip is surrounded by air or placed over a fat tissue layer, in which the simultaneous unipolar mode is the only way of creating transmural lesions. The results also suggest that the orientation of the catheter tip, i.e.

perpendicular vs. parallel, on the epicardial surface during ventricular free wall bipolar ablation does not result in significantly different lesion shapes and dimensions.

Acknowledgments

This work received financial support from the Spanish "Plan Nacional de I+D+I del Ministerio de Ciencia e Innovación" (Grant No. TEC2011-27133-C02-01), and from Universitat Politècnica de València (PAID-06-11 Ref. 1988). A. González-Suárez is the recipient of a Grant VaLi+D (ACIF/2011/194) from the Generalitat Valenciana (Spain).

Declaration of Interest

The authors report no conflicts of interest.

References

1. Sivagangabalan G, Barry MA, Huang K, Lu J, Pouliopoulos J, Thomas SP, Ross DL, Thiagalingam A, Kovoor P. Bipolar ablation of the interventricular septum is more efficient at creating a transmural line than sequential unipolar ablation. Pacing Clin Electrophysiol 2010; 33(1):16–26.
2. Nagashima K, Watanabe I, Okumura Y, Ohkubo K, Kofune M, Ohya T, Kasamaki Y, Hirayama A. Lesion formation by ventricular septal ablation with irrigated electrodes: comparison of bipolar and sequential unipolar ablation. Circ J 2011; 75(3):565–570.
3. d'Avila A, Houghtaling C, Gutiérrez P, Vragovic O, Ruskin JN, Josephson ME, Reddy VY. Catheter ablation of ventricular epicardial tissue: a comparison of standard and cooled-tip radiofrequency energy. Circulation 2004; 109(19):2363-2369.
4. Dukkipati SR, d'Avila A, Soejima K, Bala R, Inada K, Singh S, Stevenson WG, Marchlinski FE, Reddy VY. Long-term outcomes of combined epicardial and endocardial ablation of monomorphic ventricular tachycardia related to hypertrophic cardiomyopathy. Circ Arrhythm Electrophysiol 2011; 4(2):185-194.
5. Sosa E, Scanavacca M, d'Avila A, Oliveira F, Ramires JA. Nonsurgical transthoracic epicardial catheter ablation to treat recurrent ventricular tachycardia occurring late after myocardial infarction. J Am Coll Cardiol 2000; 35(6):1442-1449.

6. Nagashima K, Watanabe I, Okumura Y, Sonoda K, Kofune M, Mano H, Ohkubo K, Nakai T, Kunimoto S, Kasamaki Y, Hirayama A. Epicardial ablation with irrigated electrodes: – effect of bipolar vs. unipolar ablation on lesion formation – Circ J 2012; 76(2): 322-327.
7. Berjano EJ. Theoretical modeling for radiofrequency ablation: state-of-the-art and challenges for the future. Biomed Eng Online 2006; 5:24.
8. Abraham JP, Sparrow EM. A thermal-ablation bioheat model including liquid-to-vapor phase change, pressure- and necrosis-dependent perfusion, and moisture-dependent properties. Int J Heat Mass Tran 2007; 50(13-14):2537-2544.
9. Byeongman J, Alptekin A. Prediction of the extent of thermal damage in the cornea during conductive keratoplasty. J Therm Biol 2010; 35(4):167-174.
10. Haines DE, Watson DD. Tissue heating during radiofrequency catheter ablation: a thermodynamic model and observations in isolated perfused and superfused canine right ventricular free wall. Pacing Clin Electrophysiol 1989; 12(6):962-976.
11. Zhao G, Zhang HF, Guo XJ, Luo DW, Gao DY. Effect of blood flow and metabolism on multidimensional heat transfer during cryosurgery. Med Eng Phys 2007; 29(2):205-215.
12. Chang IA. Considerations for thermal injury analysis for RF ablation devices. Open Biomed Eng J 2010; 4:3-12.
13. Chang I, Nguyen U. Thermal modelling of lesion growth with radiofrequency ablation devices Biomed Eng Online 2004; 3(1):27.
14. Whitney J, Carswell W, Rylander N. Arrhenius parameter determination as a function of heating method and cellular microenvironment based on spatial cell viability analysis. Int J Hyperthermia 2013; 29(4):281-295.
15. Pearce JA. Comparative analysis of mathematical models of cell death and thermal damage processes. Int J Hyperthermia 2013; 29(4):262-280.
16. Jacques SL, Gaeeni MO. Thermally induced changes in optical properties of heart. Proc 11th Ann Int Conf of the IEEE Eng Med Biol Soc 1989; 4:1199–1200.
17. Doss JD. Calculation of electric fields in conductive media. Med Phys 1982; 9(4):566-573.
18. Watanabe I, Nuo M, Okumura Y, Ohkubo K, Ashino S, Kofune M, Kofune T, Nakai T, Kasamaki Y, Hirayama A. Temperature-controlled cooled-tip radiofrequency ablation in left ventricular myocardium. Int Heart J 2010; 51(3):193–198.

19. Yokoyama K, Nakagawa H, Wittkampf FH, Pitha JV, Lazzara R, Jackman WM. Comparison of electrode cooling between internal and open irrigation in radiofrequency ablation lesion depth and incidence of thrombus and steam pop. Circulation 2006; 113(1):11–19.
20. Kumar P, Mounsey JP, Gehi AK, Schwartz JD, Chung EH. Use of a closed loop irrigated catheter in epicardial ablation of ventricular tachycardia. J Interv Card Electrophysiol 2013; 38(1):35-42.
21. Schutt D, Berjano EJ, Haemmerich D. Effect of electrode thermal conductivity in cardiac radiofrequency catheter ablation: a computational modeling study. Int J Hyperthermia 2009; 25(2) 99–107.
22. Gopalakrishnan JA. A mathematical model for irrigated epicardial radiofrequency ablation. Ann Biomed Eng 2002; 30(7):884–893.
23. Pätz T, Körger T, Preusser T. Simulation of radiofrequency ablation including water evaporation. In: IFMBE Proceedings of the World Congress on Medical Physics and Biomedical Engineering 25/IV, 2009, 1287-1290.
24. Suárez AG, Hornero F, Berjano EJ. Mathematical modeling of epicardial RF ablation of atrial tissue with overlying epicardial fat. Open Biomed Eng J. 2010; 4:47-55.
25. Haemmerich D, Chachati L, Wright AS, Mahvi DM, Lee FT, Webster JG. Hepatic radiofrequency ablation with internally cooled probes: effect of coolant temperature on lesion size. IEEE Trans Biomed Eng 2003; 50(4):493–499.
26. Koruth JS, Dukkipati S, Miller MA, Neuzil P, d'Avila A, Reddy VY. Bipolar irrigated radiofrequency ablation: a therapeutic option for refractory intramural atrial and ventricular tachycardia circuits. Heart Rhythm 2012; 9(12):1932-1941.
27. González-Suárez A, Trujillo M, Burdío F, Andaluz A, Berjano E. Feasibility study of an internally cooled bipolar applicator for RF coagulation of hepatic tissue: Experimental and computational study. Int J Hyperthermia 2012; 28(7):663-673.
28. Agah R, Gandjbakhche AH, Motamedi M, Nossal R, Bonner RF. Dynamics of temperature dependent optical properties of tissue: dependence on thermally induced alteration. IEEE Trans Biomed Eng 1996; 43(8):839-846.
29. Haines DE. Letter by Haines regarding article "Direct measurement of the lethal isotherm for radiofrequency ablation of myocardial tissue". Circ Arrhythm Electrophysiol 2011; 4(5):e67.

30. Wood M, Goldberg S, Lau M, Goel A, Alexander D, Han F, Feinstein S. Direct measurement of the lethal isotherm for radiofrequency ablation of myocardial tissue. Circ Arrhythm Electrophysiol 2011; 4(3):373-378.
31. Jain MK, Wolf PD. A three-dimensional finite element model of radiofrequency ablation with blood flow and its experimental validation. Ann Biomed Eng 2000; 28(9): 1075-1084.

Table I. Thermal and electrical characteristics of the elements of the numerical models (data from [21-24]).

Element/Material		**σ (S/m)**	**k (W/m·K)**	**ρ (kg/m^3)**	**c (J/kg·K)**
Electrode		$4.6 \cdot 10^6$	71	21500	132
Plastic		10^{-5}	0.026	70	1045
Blood		0.99	0.54	1000	4180
Pericardial fluid (saline)		1.35	0.628	980	4184
Fat		0.025	0.20	900	2222
Cardiac tissue	Liquid phase	0.541	0.531	1060	3111
	Gas phase			370.44	2155.92

σ, electric conductivity; k, thermal conductivity; ρ, density; and c, specific heat.

Table II. Lesion dimensions (in mm) in the interventricular septum (IVS) for different septum thickness and three modes of RF ablation: bipolar mode (BM), sequential unipolar mode (SEUM) and simultaneous unipolar mode (SIUM).

Ablation Mode	IVS thickness	MW1	SW1	IW	MW2	SW2	D1	D2
BM	10	= IW	6.02	10.43	= IW	= SW1	transmural	
	12.5	8.18	5.56	7.55	= MW1	= SW1	transmural	
	15	9.51	7.28	7.06	= MW1	= SW1	transmural	
SEUM	10	6.80	5.39	3.34	9.29	7.87	transmural	
	12.5	6.39	5.14	-	8.80	7.75	3.78	5.36
	15	6.34	5.11	-	8.86	7.48	3.70	5.01
SIUM	10	= IW	8.35	11.26	= IW	= SW1	transmural	
	12.5	8.46	6.77	3.68	= MW1	= SW1	transmural	
	15	9.16	7.26	-	= MW1	= SW1	5.62	=D1

MW: maximum width; IW: intermediate width; SW: surface width; and D: depth.

1: left side and 2: right side.

Table III. Lesion dimensions (in mm) in the ventricular free wall (VFW) with the epicardial catheter surrounded by pericardial fluid for different wall thickness and three modes of RF ablation: bipolar mode (BM), sequential unipolar mode (SEUM) and simultaneous unipolar mode (SIUM).

Ablation Mode	VFW thickness	MW1	SW1	IW	MW2	SW2	D1	D2
BM	7.5	12.65	8.23	=MW1	=MW1	=MW1	transmural	
	10	13.90	8.58	=MW1	=MW1	=MW1	transmural	
	12.5	11.38	8.05	11.96	13.51	=MW2	transmural	
	15	10.08	7.61	8.40	12.78	=MW2	transmural	
SEUM	7.5	6.73	5.79	6.07	11.61	10.48	transmural	
	10	5.58	4.71	-	12.25	11.67	3.29	5.58
	12.5	5.72	5.12	-	12.58	12.10	3.36	5.72
	15	6.72	5.72	-	12.47	12.03	3.90	4.68
SIUM	7.5	11.67	7.35	=MW1	16.65	=MW2	transmural	
	10	7.52	9.74	11.38	17.67	=MW2	transmural	
	12.5	7.41	6.02	4.13	16.45	=MW2	transmural	
	15	7.79	6.82	-	16.01	=MW2	4.81	5.53

MW: maximum width; IW: intermediate width; SW: surface width; and D: depth.

1: left side and 2: right side.

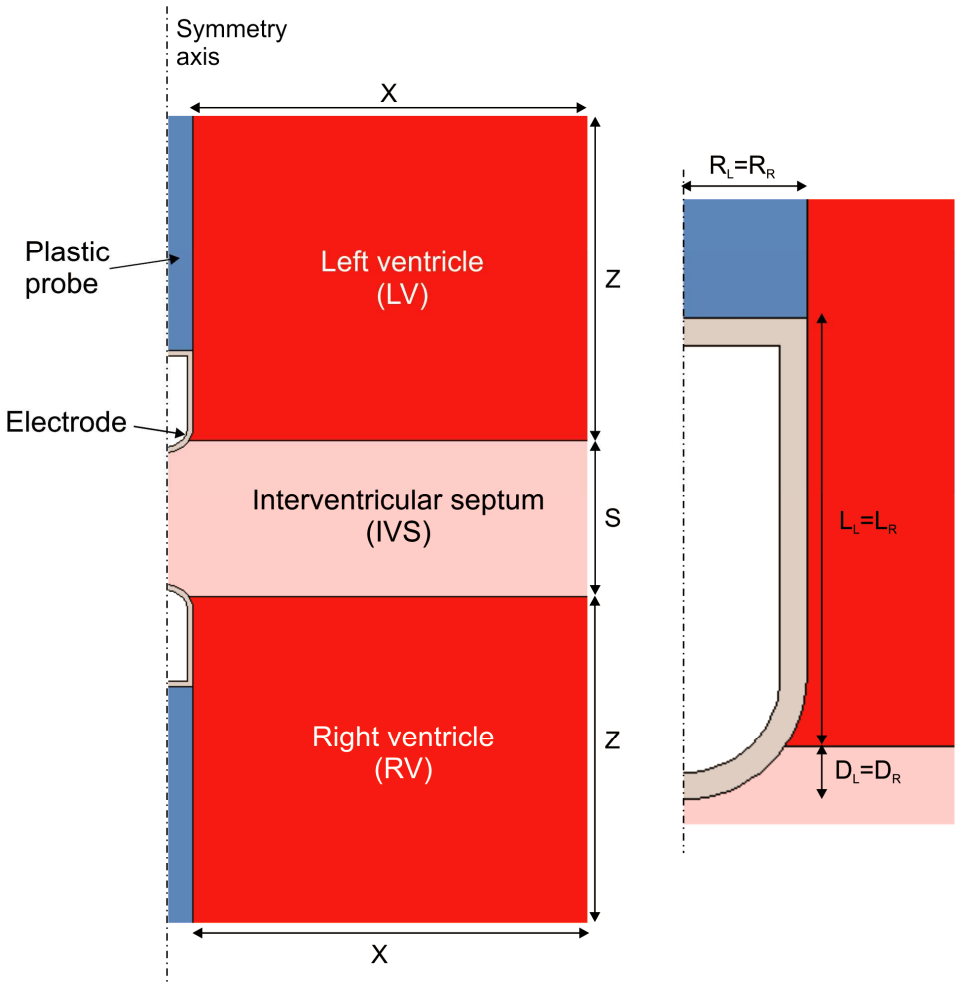

Figure 1. Left: Geometry of the computational model for interventricular septum (IVS) ablation. Septum thickness: S. The geometry of the model for ventricular free wall (VFW) ablation was similar, but circulating blood in one ventricle was replaced by pericardial fluid or air. Ventricle dimensions X and Z were obtained from a convergence test. Right: Detail of the electrode on the tissue. Electrode radius: R_L = R_R= 1.155 mm (7 Fr), electrode lengths: L_L = L_R = 3.5 mm (0.25 mm thickness wall), and insertion depth: D_L = D_R= 0.5 mm.

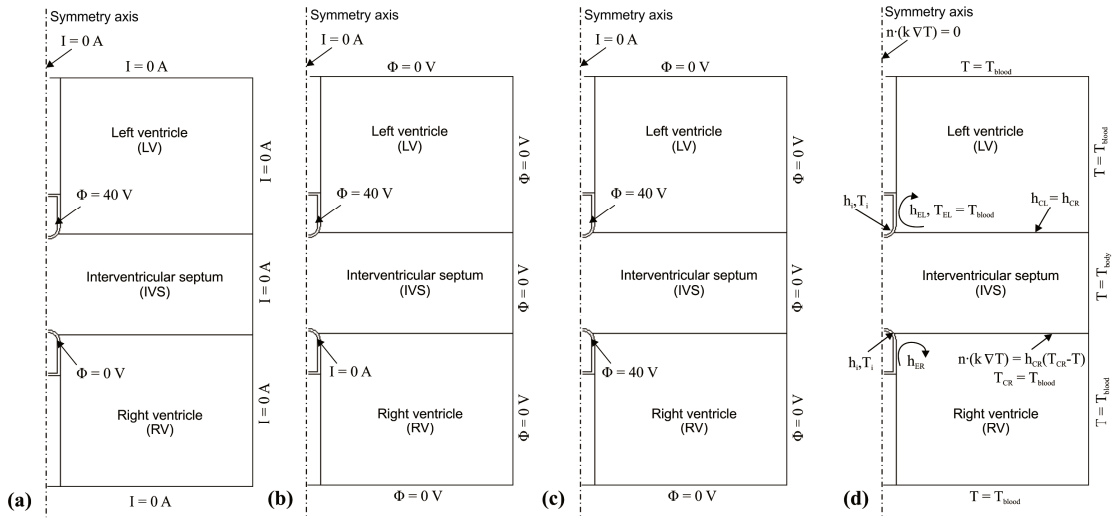

Figure 2. Electrical boundary conditions of the model for interventricular septum (IVS) ablation for **(a)** bipolar mode (BM), **(b)** sequential unipolar mode (SEUM) and **(c)** simultaneus unipolar mode (SIUM). **(d)** Thermal boundary conditions for all cases. $h_{CL} = h_{CR}$ and $h_{EL} = h_{ER}$ are the thermal transfer coefficients at the endocardium–blood and the electrode–blood interfaces, respectively.

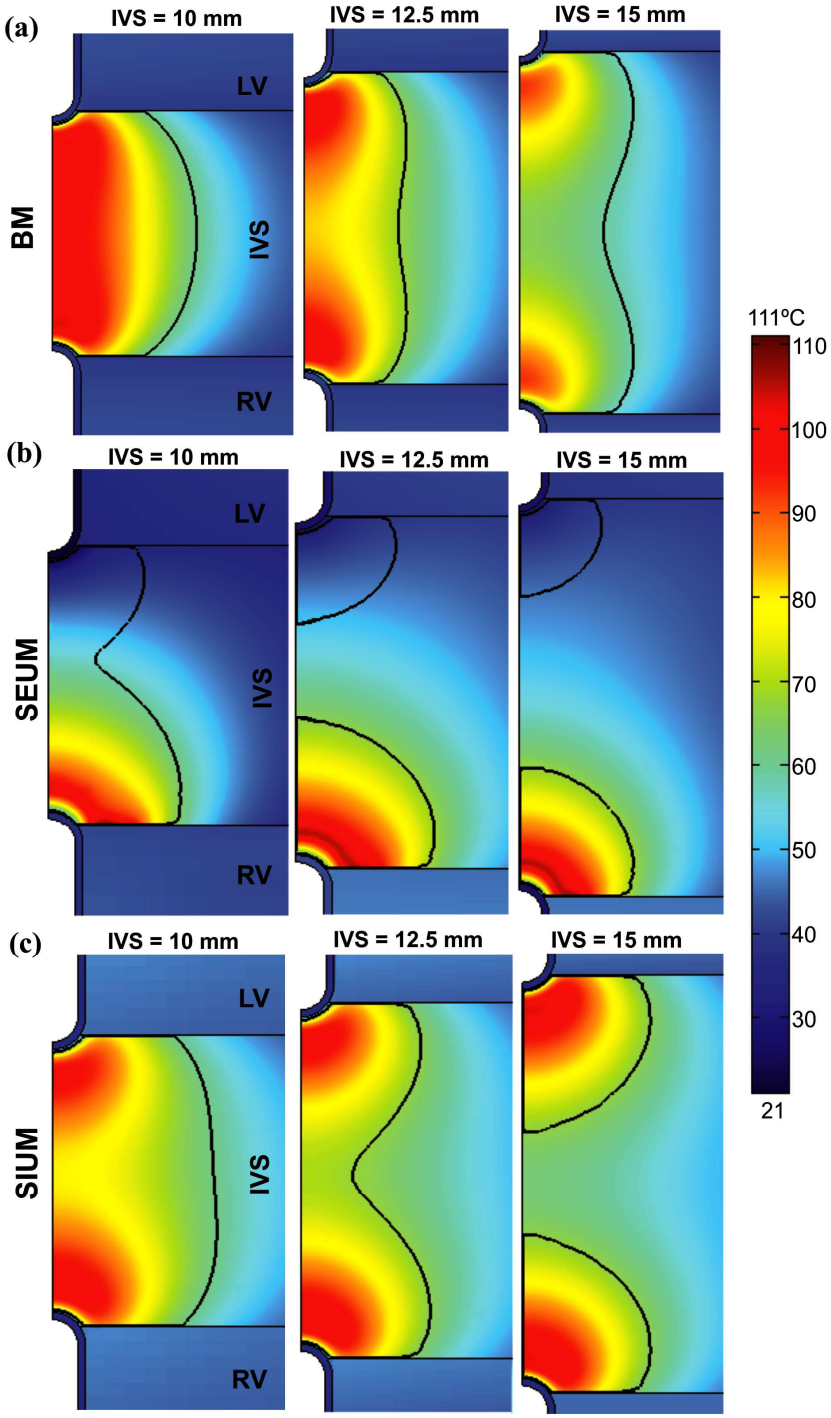

Figure 3. Temperature distribution in the tissue after 120 s of RFA across the interventricular septum (IVS) for different septum thickness from 10 to 15 mm, considering three modes of ablation: **(a)** bipolar mode (BM), **(b)** sequential unipolar mode (SEUM), and **(c)** simultaneous unipolar mode (SIUM). The solid black line is the thermal damage border (Ω =1). RL: right ventricle, and LV: left ventricle.

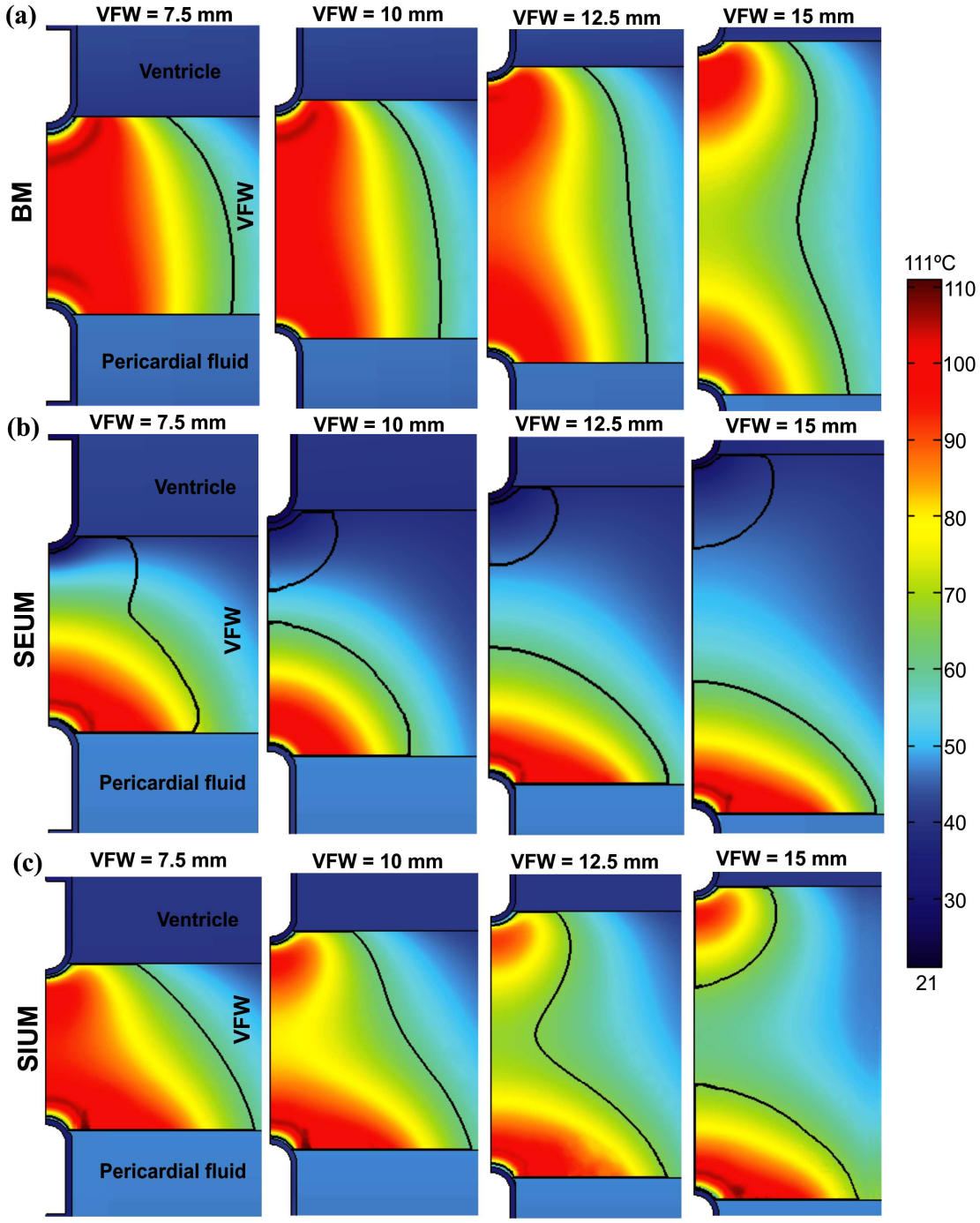

Figure 4. Temperature distribution in the tissue after 120 s of RFA across the ventricular free wall (VFW) with pericardial fluid in the epicardial space, considering different wall thickness from 7.5 to 15 mm and three modes of ablation: **(a)** bipolar mode (BM), **(b)** sequential unipolar mode (SEUM), and **(c)** simultaneous unipolar mode (SIUM). The solid black line is the thermal damage border (Ω =1).

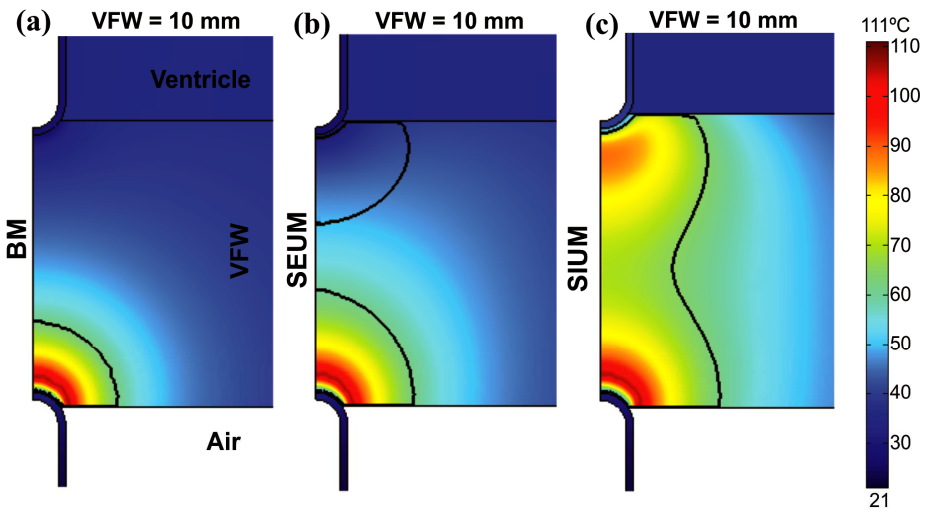

Figure 5. Temperature distributions after 120 s of RFA across the VFW (10 mm wall thickness) with the epicardial catheter surrounded by air, considering three modes of ablation: **(a)** bipolar mode (BM), **(b)** sequential unipolar mode (SEUM), and **(c)** simultaneous unipolar mode (SIUM). The solid black line is the thermal damage border (Ω =1).

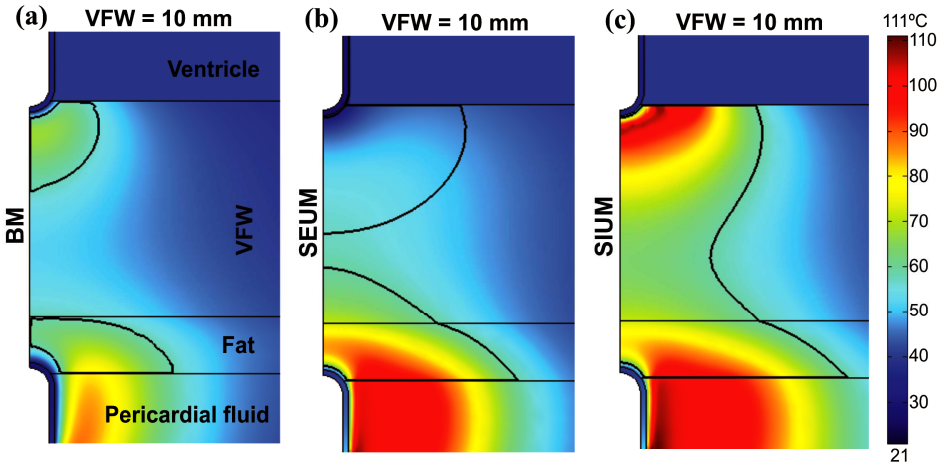

Figure 6. Temperature distributions after 120 s of RFA across the VFW (10 mm wall thickness) with the epicardial catheter placed over a fat tissue layer, considering three modes of ablation: **(a)** bipolar mode (BM), **(b)** sequential unipolar mode (SEUM), and **(c)** simultaneous unipolar mode (SIUM). The solid black line is the thermal damage border (Ω =1).

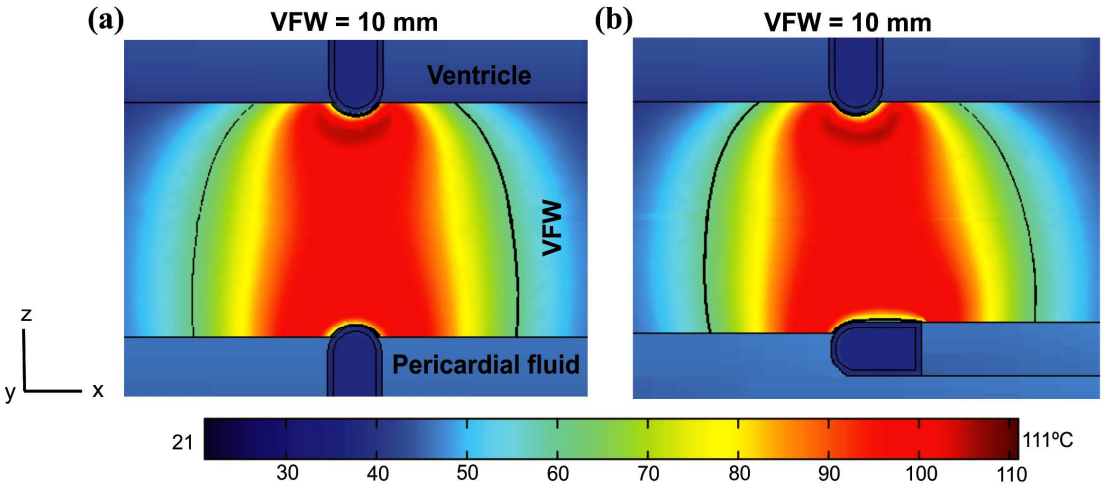

Figure 7. Temperature distributions after 120 s of RFA with BM across VFW (10 mm thickness) comparing two orientations of the epicardial catheter: **(a)** perpendicular and **(b)** parallel to the epicardium. The solid black line is the thermal damage border (Ω =1).

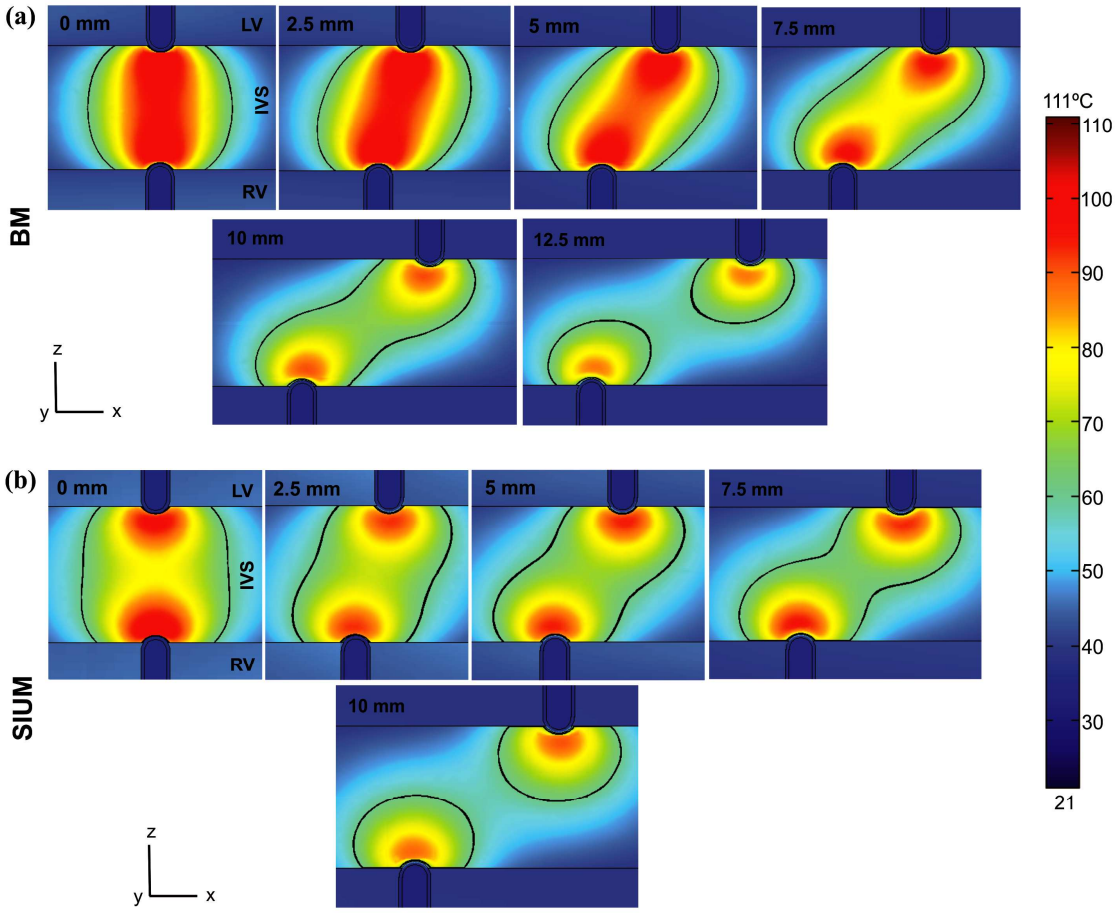

Figure 8. Temperature distributions in the tissue after 120 s of RFA with BM **(a)** and SIUM **(b)** across the IVS (10 mm thickness), increasing the misalignment between catheters in steps of 2.5 mm until the lesion was no longer transmural. Note that the lesions were transmural when they reached all the tissue at a plane of the wall, including the center. The solid black line is the thermal damage border (Ω =1). LV: left ventricle, and RV: right ventricle.

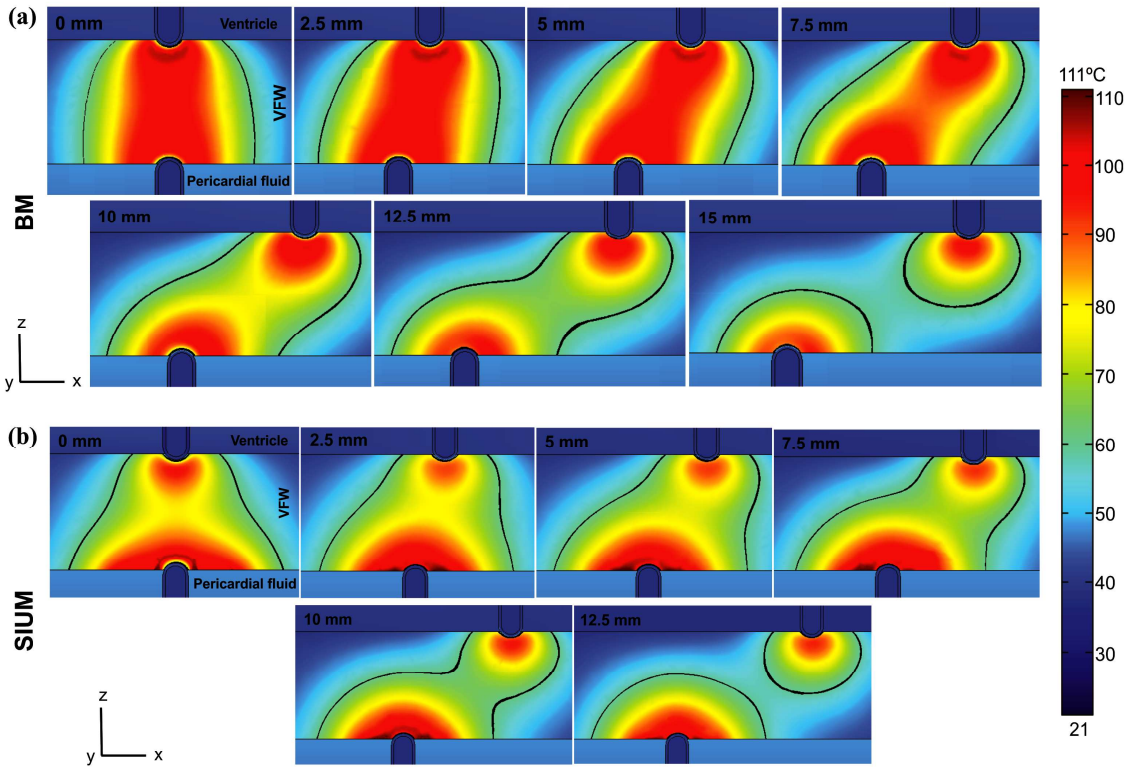

Figure 9. Temperature distributions in the tissue after 120 s of RFA with BM **(a)** and SIUM **(b)** across the VFW (10 mm thickness), increasing the misalignment between catheters in steps of 2.5 mm until the lesion was no longer transmural. The solid black line is the thermal damage border (Ω =1).

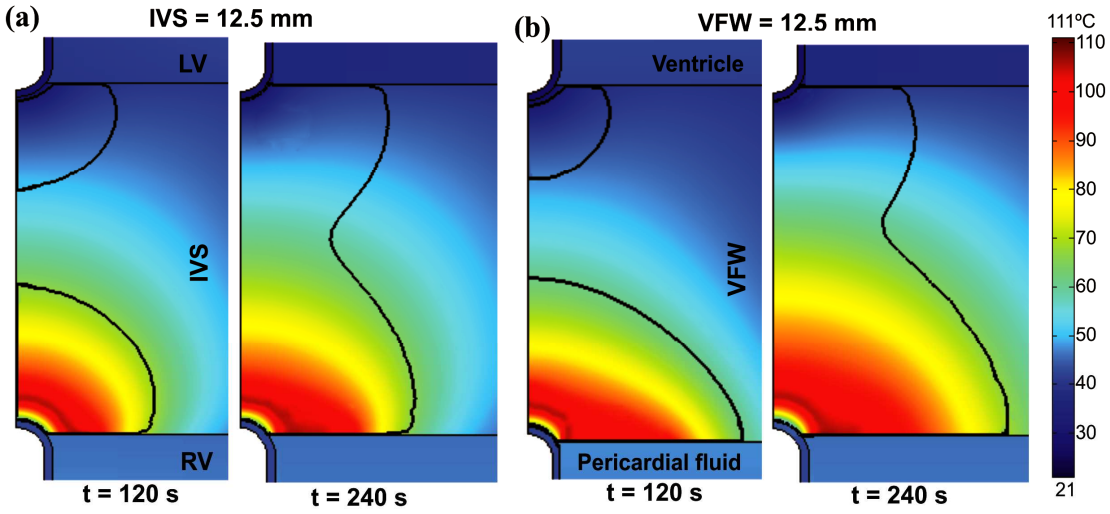

Figure 10. Temperature distributions in the tissue after 120 s and 240 s of RFA with SEUM across the IVS **(a)** and the VFW (both 12.5 mm thickness). The solid black line is the thermal damage border (Ω =1).